

Study of the Processes  $e^+e^- \rightarrow \eta\gamma$ ,  $\pi^0\gamma \rightarrow 3\gamma$  in the  
c.m. Energy Range 600–1380 MeV at CMD-2

R.R. Akhmetshin <sup>a</sup>, V.M. Aulchenko <sup>a,c</sup>, V.Sh. Banzarov <sup>a</sup>,  
A. Baratt <sup>d</sup>, L.M. Barkov <sup>a,c</sup>, N.S. Bashtovoy <sup>a</sup>, A.E. Bondar <sup>a,c</sup>,  
D.V. Bondarev <sup>a</sup>, A.V. Bragin <sup>a</sup>, S.I. Eidelman <sup>a,c</sup>,  
D.A. Epifanov <sup>a</sup>, G.V. Fedotovitch <sup>a,c</sup>, N.I. Gabyshev <sup>a</sup>,  
D.A. Gorbachev <sup>a</sup>, A.A. Grebeniuk <sup>a</sup>, D.N. Grigoriev <sup>a</sup>,  
F.V. Ignatov <sup>a</sup>, S.V. Karpov <sup>a</sup>, V.F. Kazanin <sup>a,c</sup>, B.I. Khazin <sup>a,c</sup>,  
I.A. Koop <sup>a,c</sup>, P.P. Krovovny <sup>a,c</sup>, A.S. Kuzmin <sup>a,c</sup>,  
Yu.E. Lischenko <sup>a</sup>, I.B. Logashenko <sup>a</sup>, P.A. Lukin <sup>a</sup>,  
K.Yu. Mikhailov <sup>a</sup>, A.I. Milstein <sup>a,c</sup>, I.N. Nesterenko <sup>a,c</sup>,  
V.S. Okhaphkin <sup>a</sup>, A.V. Otboev <sup>a,c</sup>, A.S. Popov <sup>a</sup>, S.I. Redin <sup>a</sup>,  
B.L. Roberts <sup>b</sup>, N.I. Root <sup>a</sup>, A.A. Ruban <sup>a</sup>, N.M. Ryskulov <sup>a</sup>,  
A.G. Shamov <sup>a</sup>, Yu.M. Shatunov <sup>a</sup>, B.A. Shwartz <sup>a,c</sup>,  
A.L. Sibidanov <sup>a,c</sup>, V.A. Sidorov <sup>a</sup>, A.N. Skrinsky <sup>a</sup>,  
I.G. Snopkov <sup>a</sup>, E.P. Solodov <sup>a,c</sup>, J.A. Thompson <sup>d 1</sup>,  
A.A. Valishev <sup>a</sup>, Yu.V. Yudin <sup>a</sup>, A.S. Zaitsev <sup>a,c</sup>, S.G. Zverev <sup>a</sup>

<sup>a</sup>*Budker Institute of Nuclear Physics, Novosibirsk, 630090, Russia*

<sup>b</sup>*Boston University, Boston, MA 02215, USA*

<sup>c</sup>*Novosibirsk State University, Novosibirsk, 630090, Russia*

<sup>d</sup>*University of Pittsburgh, Pittsburgh, PA 15260, USA*

<sup>e</sup>*Yale University, New Haven, CT 06511, USA*

---

<sup>1</sup> deceased

---

**Abstract**

The processes  $e^+e^- \rightarrow \eta\gamma$ ,  $\pi^0\gamma \rightarrow 3\gamma$  have been studied in the c.m. energy range 600–1380 MeV with the CMD-2 detector. The following branching ratios have been determined:

$$\begin{aligned}\mathcal{B}(\rho^0 \rightarrow \eta\gamma) &= (3.21 \pm 1.39 \pm 0.20) \cdot 10^{-4}, \\ \mathcal{B}(\omega \rightarrow \eta\gamma) &= (4.44_{-1.83}^{+2.59} \pm 0.28) \cdot 10^{-4}, \\ \mathcal{B}(\phi \rightarrow \eta\gamma) &= (1.373 \pm 0.014 \pm 0.085) \cdot 10^{-2}, \\ \mathcal{B}(\rho^0 \rightarrow \pi^0\gamma) &= (6.21_{-1.18}^{+1.28} \pm 0.39) \cdot 10^{-4}, \\ \mathcal{B}(\omega \rightarrow \pi^0\gamma) &= (9.06 \pm 0.20 \pm 0.57) \cdot 10^{-2}, \\ \mathcal{B}(\phi \rightarrow \pi^0\gamma) &= (1.258 \pm 0.037 \pm 0.077) \cdot 10^{-3}.\end{aligned}$$

---

## 1 Introduction

The magnetic dipole transitions of the light vector mesons ( $\rho$ ,  $\omega$  and  $\phi$ ) to the  $\pi^0\gamma$  and  $\eta\gamma$  final states have traditionally provided a convenient laboratory for various tests of theoretical concepts, particularly the nonrelativistic quark model and Vector Dominance Model (VDM) [1,2]. There are ongoing discussions about mechanisms of SU(3) breaking, possible admixture of glue in mesons and the role of anomalies in radiative decays [3,4,5,6,7,8]. Precise measurements of the cross sections of  $e^+e^-$  annihilation into the  $\pi^0\gamma$  and  $\eta\gamma$  final states in the broad c.m.energy range are necessary for the problem of the muon anomaly [9]. Radiative decays to  $\pi^0\gamma$  and  $\eta\gamma$  can also provide important information on the properties of the  $\rho$ ,  $\omega$  and  $\phi$  excitations as well as on the existence of light hybrids between 1000 and 2000 MeV [10,11].

Despite previous experimental efforts (cf. the detailed bibliography in [12]), of these decays only  $\omega \rightarrow \pi^0\gamma$  and  $\phi \rightarrow \eta\gamma$  are rather well studied. A three-photon final state is convenient for the investigation of the  $\pi^0\gamma$  and  $\eta\gamma$  final states since both  $\pi^0$  and  $\eta$  readily decay into two photons. Measurements of the branching ratios for corresponding decays of the  $\rho$ ,  $\omega$  and  $\phi$  using the two-photon decay mode have been performed at ND [13,14] and SND [15,16], however, none of them covered the whole off-resonance energy range.

In this work we report on the measurement of the cross section of the processes  $e^+e^- \rightarrow \pi^0\gamma$  and  $e^+e^- \rightarrow \eta\gamma$  in the three-photon final state in the c.m.energy range 600–1380 MeV using the data from the CMD-2 detector at the VEPP-

2M  $e^+e^-$  collider.

## 2 Experiment

The general purpose detector CMD-2 has been described in detail elsewhere [17]. Its tracking system consists of a cylindrical drift chamber (DC) and double-layer multiwire proportional Z-chamber, both also used for the trigger, and both inside a thin ( $0.38 X_0$ ) superconducting solenoid with a field of 1 T. The barrel CsI calorimeter (BC) with a thickness of  $8.1 X_0$  placed outside the solenoid has energy resolution for photons of about 9% in the energy range from 100 to 700 MeV. The angular resolution is of the order of 0.02 radians. The end-cap BGO calorimeter with a thickness of  $13.4 X_0$  placed inside the solenoid has energy and angular resolution varying from 9% to 4% and from 0.03 to 0.02 radians, respectively, for the photon energy in the range 100 to 700 MeV. The barrel and end-cap calorimeter systems cover a solid angle of  $0.92 \times 4\pi$  radians.

This analysis is based on a data sample corresponding to integrated luminosity of  $21 \text{ pb}^{-1}$  collected in 1997–1998 in the energy range 600–1380 MeV. The step of the c.m. energy scan varied from 0.5 MeV near the  $\omega$  and  $\phi$  peaks to 10 MeV far from the resonances. The beam energy spread is about  $4 \times 10^{-4}$  of the total energy. The luminosity is measured using events of Bhabha scattering at large angles [18].

A GEANT3 based Monte Carlo simulation (MC) package is used to model the detector response and determine the efficiency [19]. Because of the beam induced background additional (“fake”) clusters can appear in the calorimeter. To take this effect into account in MC we determine a corresponding probability as well as photon energy and angular spectra directly from the data using the process  $e^+e^- \rightarrow \pi^+\pi^-\pi^0$ , and then include generation of such photons in the detector response during simulation.

## 3 Data analysis

At the initial stage, events are selected which have no tracks in the DC, three or four photons in the CsI calorimeter, the total energy deposition  $0.8 < E_{\text{tot}}/E_{\text{cm}} < 1.1$ , the total momentum  $P_{\text{tot}}/E_{\text{cm}} < 0.15$  and the minimum photon energy of 50 MeV. Figure 1 (left) shows the  $E_{\text{tot}}$  distribution for the data and signal MC near the  $\phi$  resonance. One can see good agreement between

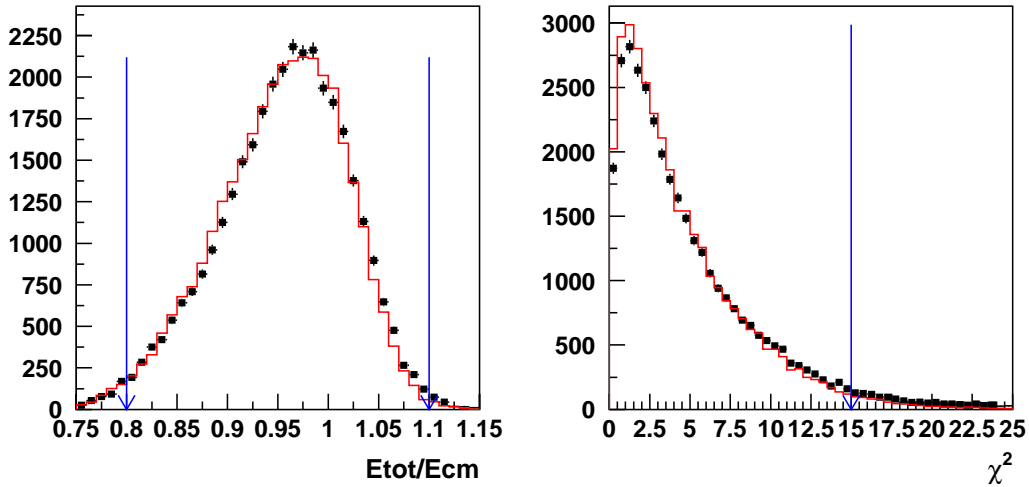


Fig. 1. The  $E_{\text{tot}}/E_{\text{cm}}$  (left) and  $\chi^2$  (right) distributions. The points with error bars represent experimental events, the histograms show the MC simulation. The arrows indicate the cuts imposed.

the data and signal MC. About  $52 \times 10^3$  events were selected in the whole energy range after these requirements.

Then a kinematic fit requiring energy-momentum conservation (a standard 4C fit) was performed. We require  $\chi^2 < 15$  that provides a good signal/noise ratio while the number of rejected signal events is still small (see Fig. 1).

The reconstruction procedure assumes three photons, i.e., for events with four photons a combination of three photons with the minimum  $\chi^2$  is chosen. After this stage about  $48 \times 10^3$  events remain.

The dominant background comes from the QED three-photon annihilation:  $e^+e^- \rightarrow 3\gamma$ . These events can not be completely rejected by selection criteria. The  $\eta\gamma$ ,  $\pi^0\gamma$  and background events can be separated using decay dynamics. To this end two methods were considered: Dalitz plot analysis and a fit of the two-photon invariant mass distributions.

Figure 2 shows the Dalitz plot for the  $3\gamma$  final state in the  $\phi$  meson energy range ( $1011.4 \text{ MeV} < E_{\text{CM}} < 1027.4 \text{ MeV}$ ). Here the photons are sorted by their energy so that the first photon has a maximum energy:  $E_1 > E_2 > E_3$ . The Dalitz plot is divided into three regions:  $D_{\eta\gamma}$  ( $340 \text{ MeV} < E_2 < 385 \text{ MeV}$  or  $E_1 < 385 \text{ MeV}$ ),  $D_{\pi^0\gamma}$  ( $491 \text{ MeV} < E_1 < 511 \text{ MeV}$ ) and  $D_{\text{bg}}$  (all the remaining events). For each of the three final states ( $\eta\gamma$ ,  $\pi^0\gamma$  and QED) we determine from the MC simulation the probabilities to enter each region. Based on that, from the population of various regions of the Dalitz plot in the data the total number of events due to each process is calculated. However, this method can provide bias in the signal yield determination because of the possible deviation

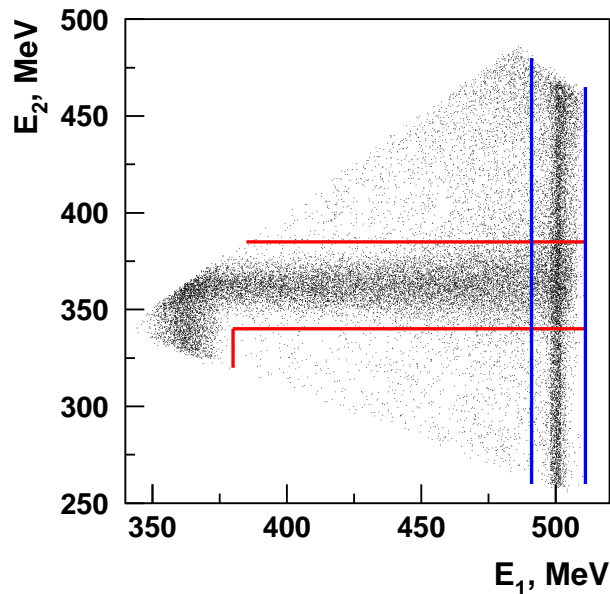


Fig. 2. The Dalitz plot for the  $3\gamma$  final state at the  $\phi$  meson energy. The points represent experimental events, the lines indicate boundaries used in the selection criteria, see the text for more detail.

between the signal shape in the data and MC simulation. Additional bias can arise from the background processes of the non-QED origin.

Therefore, we obtain the number of  $\eta\gamma$  and  $\pi^0\gamma$  events by fitting the two-photon invariant mass distribution. In this method the signal shape is obtained from the data decreasing a possible bias. The difference in the number of selected events in these two methods (about 3%) was considered as a systematic uncertainty because of the separation procedure.

For  $\pi^0$  reconstruction the invariant mass of the two softer photons ( $M_{23}$ ) is used. For the  $\eta$  signal three combinations are used:

- (1) In case of  $E_1 < m_\eta^2/\sqrt{s}$ , two hard photons are used ( $M_{12}$ ).
- (2) Otherwise, if  $E_3 < m_\eta^2/\sqrt{s}$ , we use the first and third photons ( $M_{13}$ ).
- (3) In other cases two soft photons ( $M_{23}$ ) are used.

Figure 3 shows the two-photon invariant mass distributions for the  $\pi^0$  (left) and  $\eta$  (right) combinations near the peak of the  $\phi$  meson.

Other possible sources of background are the processes  $e^+e^- \rightarrow \eta\gamma \rightarrow 3\pi^0\gamma$ ,  $e^+e^- \rightarrow K_S K_L$ ,  $e^+e^- \rightarrow \gamma\gamma$  and  $e^+e^- \rightarrow \omega\pi^0 \rightarrow \pi^0\pi^0\gamma$ . The expected number of events from these processes was calculated from the detection efficiencies determined by the MC simulation and their cross sections independently measured at CMD-2 [20,21,22,23,24]. The fraction of background events is negligible below the  $\phi$  meson and is about 2% only in the  $\phi$  meson energy range.

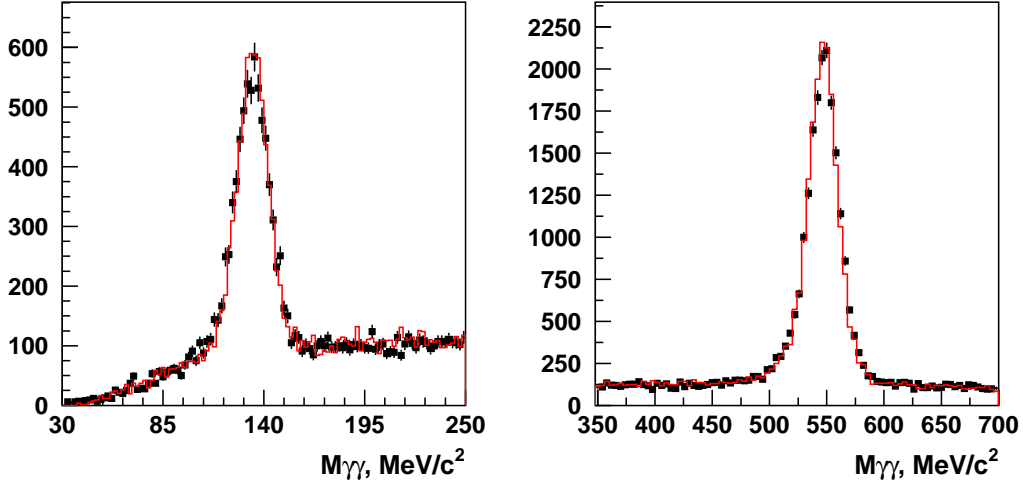


Fig. 3. The two-photon invariant mass distributions in the  $\pi^0$  (left) and  $\eta$  (right) mass range. The points with error bars represent experimental events, histograms show the MC simulation.

Above the  $\phi$  meson the expected cross section of the signal is very low (0.01–0.1 nb) and that of the background remaining after all selection criteria has close or even higher value. The separation procedure gives 17400  $\eta\gamma$  events, 18680  $\pi^0\gamma$  events and about 12000 QED events in the whole energy range considered.

### 3.1 Approximation of the cross sections

At each energy point  $i$  the cross section of the process  $\sigma_i$  of a given process is calculated using the following formula:

$$\sigma_i = \frac{N_i}{L_i \varepsilon_i (1 + \delta_i)}, \quad (1)$$

where  $N_i$  is the number of selected events,  $L_i$  is the integrated luminosity,  $\varepsilon_i$  is the detection efficiency and  $(1 + \delta_i)$  is the radiative correction at the  $i$ -th energy point.

The detection efficiency was calculated from the Monte Carlo simulation taking into account corrections obtained from the data and the neutral trigger efficiency. The neutral trigger (NT) is part of the CMD-2 trigger system responsible for events with a final state of photons only, without any charged tracks. The NT efficiency was estimated using events of the process  $e^+e^- \rightarrow e^+e^-\gamma$  at each energy point. Its value varied from about 80% to 90%.

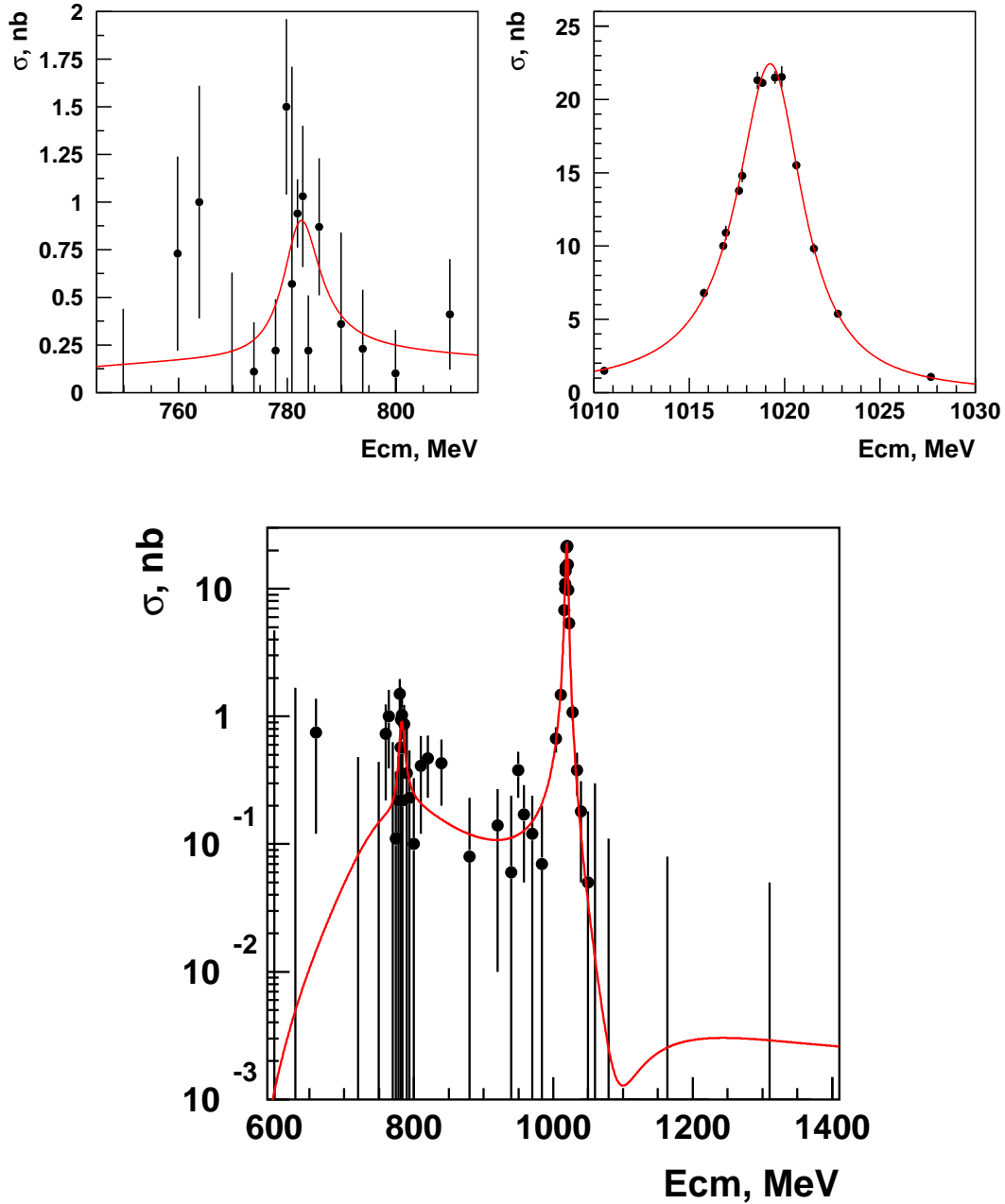


Fig. 4. The cross section of the process  $e^+e^- \rightarrow \eta\gamma$ . The points with error bars represent the experimental data, the curve corresponds to the result of the fit.

The radiative corrections are calculated according to [25]. The dependence of the detection efficiency on the energy of the emitted photon is determined from simulation.

The obtained cross sections of the processes  $e^+e^- \rightarrow \eta\gamma, \pi^0\gamma$  are shown in Figs. 4, 5. The observed pattern of the energy dependence is due to the interference of the  $\rho, \omega$  and  $\phi$  mesons. The detailed information on this analysis is

Table 1

The c.m. energy, integrated luminosity, number of selected events, detection efficiency, radiative correction, and Born cross section  $\sigma$  of the process  $e^+e^- \rightarrow \eta\gamma$ .

$\sqrt{s}$ , MeV	$L$ , nb $^{-1}$	$N_{\text{exp}}$	$\varepsilon$ , %	$1 + \delta$	$\sigma$ , nb
599.86	35.2	$0.1 \pm 2.3$	2.3	-0.157	$< 4.71$
629.86	44.6	$0.7 \pm 2.8$	7.2	-0.142	$< 1.68$
659.86	39.8	$3.0 \pm 2.9$	11.6	-0.134	$0.75 \pm 0.63$
719.86	56.9	$0.0 \pm 2.5$	15.0	-0.126	$< 0.48$
749.86	42.9	$0.1 \pm 1.9$	16.0	-0.117	$< 0.44$
759.86	33.7	$3.4 \pm 2.7$	15.7	-0.115	$0.73 \pm 0.51$
763.86	39.7	$5.6 \pm 3.9$	16.0	-0.116	$1.00 \pm 0.61$
769.86	34.3	$0.2 \pm 2.1$	17.0	-0.126	$< 0.63$
773.86	70.1	$1.0 \pm 2.8$	15.8	-0.147	$0.11 \pm 0.26$
777.86	83.6	$2.4 \pm 3.5$	15.8	-0.186	$0.22 \pm 0.27$
779.86	56.6	$10.0 \pm 3.9$	14.7	-0.204	$1.50 \pm 0.46$
780.86	58.5	$2.3 \pm 5.9$	8.8	-0.207	$0.57 \pm 1.14$
781.86	366.8	$41.2 \pm 9.3$	14.7	-0.203	$0.94 \pm 0.18$
782.86	77.6	$9.8 \pm 4.4$	15.3	-0.191	$1.03 \pm 0.37$
783.86	71.7	$2.1 \pm 3.3$	15.7	-0.172	$0.22 \pm 0.29$
785.86	67.0	$8.2 \pm 3.9$	16.0	-0.123	$0.87 \pm 0.36$
789.86	28.4	$1.5 \pm 2.1$	15.2	-0.046	$0.36 \pm 0.48$
793.86	46.2	$1.7 \pm 2.2$	15.9	-0.010	$0.23 \pm 0.31$
799.86	56.5	$0.9 \pm 2.0$	15.5	0.005	$0.10 \pm 0.23$
809.86	59.9	$3.9 \pm 2.7$	15.9	0.006	$0.41 \pm 0.29$
819.86	109.4	$8.0 \pm 4.1$	15.8	0.004	$0.47 \pm 0.24$
839.86	130.4	$8.6 \pm 4.5$	15.4	-0.006	$0.43 \pm 0.23$
879.86	167.9	$2.1 \pm 3.9$	15.2	-0.037	$0.08 \pm 0.15$
919.86	285.4	$5.7 \pm 5.4$	15.0	-0.063	$0.14 \pm 0.13$
939.86	136.7	$1.1 \pm 3.8$	15.5	-0.077	$0.06 \pm 0.18$
949.86	226.1	$12.5 \pm 5.5$	16.2	-0.085	$0.38 \pm 0.15$
957.86	250.1	$6.2 \pm 4.7$	16.5	-0.093	$0.17 \pm 0.12$
969.86	249.7	$4.7 \pm 5.1$	17.2	-0.108	$0.12 \pm 0.12$
983.93	307.7	$5.2 \pm 7.0$	20.4	-0.132	$0.07 \pm 0.13$



Table 2

The c.m. energy, integrated luminosity, number of selected events, detection efficiency, radiative correction, and Born cross section  $\sigma$  of the process  $e^+e^- \rightarrow \eta\gamma$ .

$\sqrt{s}$ , MeV	$L$ , nb $^{-1}$	$N_{\text{exp}}$	$\varepsilon$ , %	$1 + \delta$	$\sigma$ , nb
1003.91	357.7	$44.0 \pm 10.2$	20.3	-0.192	$0.67 \pm 0.15$
1010.53	477.3	$109.6 \pm 14.9$	19.9	-0.227	$1.48 \pm 0.16$
1015.77	391.7	$401.3 \pm 23.0$	20.0	-0.268	$6.80 \pm 0.30$
1016.77	660.1	$968.1 \pm 34.8$	19.6	-0.277	$10.00 \pm 0.27$
1016.91	306.1	$497.6 \pm 24.9$	20.0	-0.277	$10.90 \pm 0.49$
1017.61	673.7	$1362.1 \pm 40.8$	20.1	-0.282	$13.77 \pm 0.32$
1017.77	563.1	$1198.8 \pm 38.2$	19.9	-0.282	$14.80 \pm 0.44$
1018.58	410.1	$1230.8 \pm 38.4$	20.1	-0.278	$21.31 \pm 0.58$
1018.83	977.5	$2855.9 \pm 57.8$	19.9	-0.274	$21.13 \pm 0.30$
1019.50	633.1	$1941.9 \pm 47.5$	20.1	-0.254	$21.50 \pm 0.43$
1019.84	810.8	$2584.6 \pm 54.6$	20.2	-0.238	$21.54 \pm 0.73$
1020.62	876.3	$2231.7 \pm 51.3$	20.0	-0.187	$15.52 \pm 0.30$
1021.54	440.6	$800.5 \pm 30.9$	20.0	-0.112	$9.82 \pm 0.36$
1022.79	551.0	$621.5 \pm 28.0$	20.1	0.007	$5.38 \pm 0.26$
1027.67	562.2	$198.9 \pm 17.3$	20.2	0.591	$1.08 \pm 0.15$
1033.67	510.8	$100.0 \pm 14.0$	19.9	1.557	$0.38 \pm 0.14$
1039.59	447.5	$66.5 \pm 11.9$	20.1	2.911	$0.18 \pm 0.13$
1049.80	312.5	$23.4 \pm 8.2$	19.6	6.778	$0.05 \pm 0.13$
1059.49	220.6	$9.8 \pm 5.9$	19.3	13.272	$< 0.30$
1079.00	437.0	$4.6 \pm 6.8$	22.7	39.899	$< 0.11$
1163.40	918.2	$0.0 \pm 10.3$	21.8	0.035	$< 0.08$
1310.00	4249.0	$-0.4 \pm 21.6$	20.9	-0.074	$< 0.05$

listed in Tables 1-4. The cross section shown there is a so called “dressed” one, which is used in the approximation of the energy dependence with resonances. For applications to various dispersion integrals like that for the leading order hadronic contribution to the muon anomalous magnetic moment, the “bare” cross section should be used [26].

The maximum likelihood method is applied to fit the energy dependence of the experimental cross sections obtained from the relation (1).

Table 3

The c.m. energy, integrated luminosity, number of selected events, detection efficiency, radiative correction, and Born cross section  $\sigma$  of the process  $e^+e^- \rightarrow \pi^0\gamma$ .

$\sqrt{s}$ , MeV	$L$ , nb $^{-1}$	$N_{\text{exp}}$	$\varepsilon$ , %	$1 + \delta$	$\sigma$ , nb
599.86	35.2	$4.8 \pm 3.6$	12.0	-0.089	$1.23 \pm 0.86$
629.86	44.6	$9.2 \pm 4.2$	12.8	-0.093	$1.78 \pm 0.74$
659.86	39.8	$8.6 \pm 4.4$	12.5	-0.099	$1.92 \pm 0.89$
719.86	56.9	$14.1 \pm 5.2$	14.0	-0.112	$2.00 \pm 0.65$
749.86	42.9	$27.1 \pm 5.9$	14.3	-0.131	$5.08 \pm 0.97$
759.86	33.7	$35.0 \pm 6.8$	14.7	-0.150	$8.31 \pm 1.40$
763.86	39.7	$62.8 \pm 8.6$	14.5	-0.162	$12.97 \pm 1.52$
769.86	34.3	$76.7 \pm 9.2$	15.5	-0.185	$17.64 \pm 1.77$
773.86	70.1	$281.1 \pm 17.3$	14.6	-0.204	$34.33 \pm 1.82$
777.86	83.6	$721.5 \pm 27.5$	14.4	-0.224	$76.65 \pm 2.64$
779.86	56.6	$757.7 \pm 27.8$	13.8	-0.229	$125.81 \pm 4.92$
780.86	58.5	$717.7 \pm 27.0$	8.6	-0.228	$184.98 \pm 10.99$
781.86	366.8	$6619.7 \pm 82.0$	13.6	-0.221	$172.26 \pm 2.47$
782.86	77.6	$1664.6 \pm 41.1$	14.9	-0.206	$183.37 \pm 4.80$
783.86	71.7	$1403.6 \pm 37.7$	14.9	-0.183	$162.00 \pm 4.72$
785.86	67.0	$978.8 \pm 31.6$	13.9	-0.116	$118.44 \pm 4.16$
789.86	28.4	$187.8 \pm 13.9$	14.6	0.050	$42.80 \pm 3.80$
793.86	46.2	$166.2 \pm 13.3$	14.8	0.217	$19.93 \pm 2.06$
799.86	56.5	$134.8 \pm 12.2$	14.8	0.441	$11.18 \pm 1.52$
809.86	59.9	$83.7 \pm 9.9$	15.5	0.724	$5.22 \pm 1.09$
819.86	109.4	$87.9 \pm 10.4$	15.4	0.906	$2.74 \pm 0.62$
839.86	130.4	$61.7 \pm 9.2$	15.8	0.901	$1.58 \pm 0.45$
879.86	167.9	$17.2 \pm 6.0$	17.2	0.342	$0.44 \pm 0.21$
919.86	285.4	$20.8 \pm 6.6$	17.4	0.021	$0.41 \pm 0.13$
939.86	136.7	$18.0 \pm 5.5$	17.9	0.001	$0.74 \pm 0.22$
949.86	226.1	$20.1 \pm 6.2$	18.0	-0.008	$0.50 \pm 0.15$
957.86	250.1	$15.7 \pm 5.8$	18.4	-0.015	$0.35 \pm 0.13$
969.86	249.7	$11.8 \pm 5.4$	18.6	-0.029	$0.26 \pm 0.12$
983.93	307.7	$9.4 \pm 6.3$	19.9	-0.053	$0.16 \pm 0.11$

Table 4

The c.m. energy, integrated luminosity, number of selected events, detection efficiency, radiative correction, and Born cross section  $\sigma$  of the process  $e^+e^- \rightarrow \pi^0\gamma$ .

$\sqrt{s}$ , MeV	$L$ , nb $^{-1}$	$N_{\text{exp}}$	$\varepsilon$ , %	$1 + \delta$	$\sigma$ , nb
1003.91	357.7	$29.5 \pm 8.2$	20.5	-0.127	$0.44 \pm 0.12$
1010.53	477.3	$50.3 \pm 10.1$	20.7	-0.179	$0.61 \pm 0.10$
1015.77	391.7	$120.9 \pm 13.3$	20.5	-0.243	$1.95 \pm 0.17$
1016.77	660.1	$306.1 \pm 20.7$	20.4	-0.256	$2.95 \pm 0.16$
1016.91	306.1	$175.4 \pm 15.3$	21.0	-0.257	$3.59 \pm 0.30$
1017.61	673.7	$401.4 \pm 23.3$	20.3	-0.263	$3.97 \pm 0.18$
1017.77	563.1	$363.4 \pm 22.0$	20.5	-0.264	$4.29 \pm 0.24$
1018.58	410.1	$347.8 \pm 21.5$	20.7	-0.260	$5.72 \pm 0.32$
1018.83	977.5	$764.3 \pm 32.1$	20.2	-0.255	$5.46 \pm 0.17$
1019.50	633.1	$466.7 \pm 25.2$	20.7	-0.228	$4.77 \pm 0.24$
1019.84	810.8	$591.8 \pm 28.5$	20.8	-0.208	$4.54 \pm 0.52$
1020.62	876.3	$454.3 \pm 26.0$	20.7	-0.139	$2.85 \pm 0.15$
1021.54	440.6	$143.4 \pm 15.2$	20.6	-0.024	$1.52 \pm 0.17$
1022.79	551.0	$114.6 \pm 14.0$	20.4	0.199	$0.78 \pm 0.13$
1027.67	562.2	$35.1 \pm 9.2$	20.6	2.660	$0.08 \pm 0.08$
1033.67	510.8	$13.8 \pm 7.5$	20.7	43.316	$< 0.11$
1039.59	447.5	$10.4 \pm 6.6$	20.7	72.963	$< 0.11$
1049.80	312.5	$1.8 \pm 5.1$	20.4	6.939	$< 0.13$
1059.49	220.6	$2.0 \pm 5.3$	20.4	3.314	$< 0.20$
1079.00	437.0	$-0.6 \pm 5.5$	27.4	1.634	$< 0.08$
1163.40	918.2	$19.8 \pm 9.7$	28.1	-0.047	$0.08 \pm 0.04$
1310.00	4249.0	$48.1 \pm 16.2$	26.9	-0.143	$0.05 \pm 0.02$

The Born cross section of these processes can be written as:

$$\sigma_{P\gamma}(s) = \frac{F_{P\gamma}(s)}{s^{3/2}} \cdot \left| \sum_V A_V \right|^2, \quad (2)$$

$$A_V = \sqrt{\sigma_V^{(0)} \frac{m_V^3}{F(m_V^2)}} \cdot \frac{m_V \Gamma_V e^{i\varphi_V}}{m_V^2 - s - i\sqrt{s}\Gamma_V(s)},$$

where  $m_V$  is the mass of the resonance,  $\Gamma_V(s)$  and  $\Gamma_V = \Gamma_V(m_V^2)$  are its width at the squared c.m. energy  $s$  and at the resonance peak ( $s = m_V^2$ ),

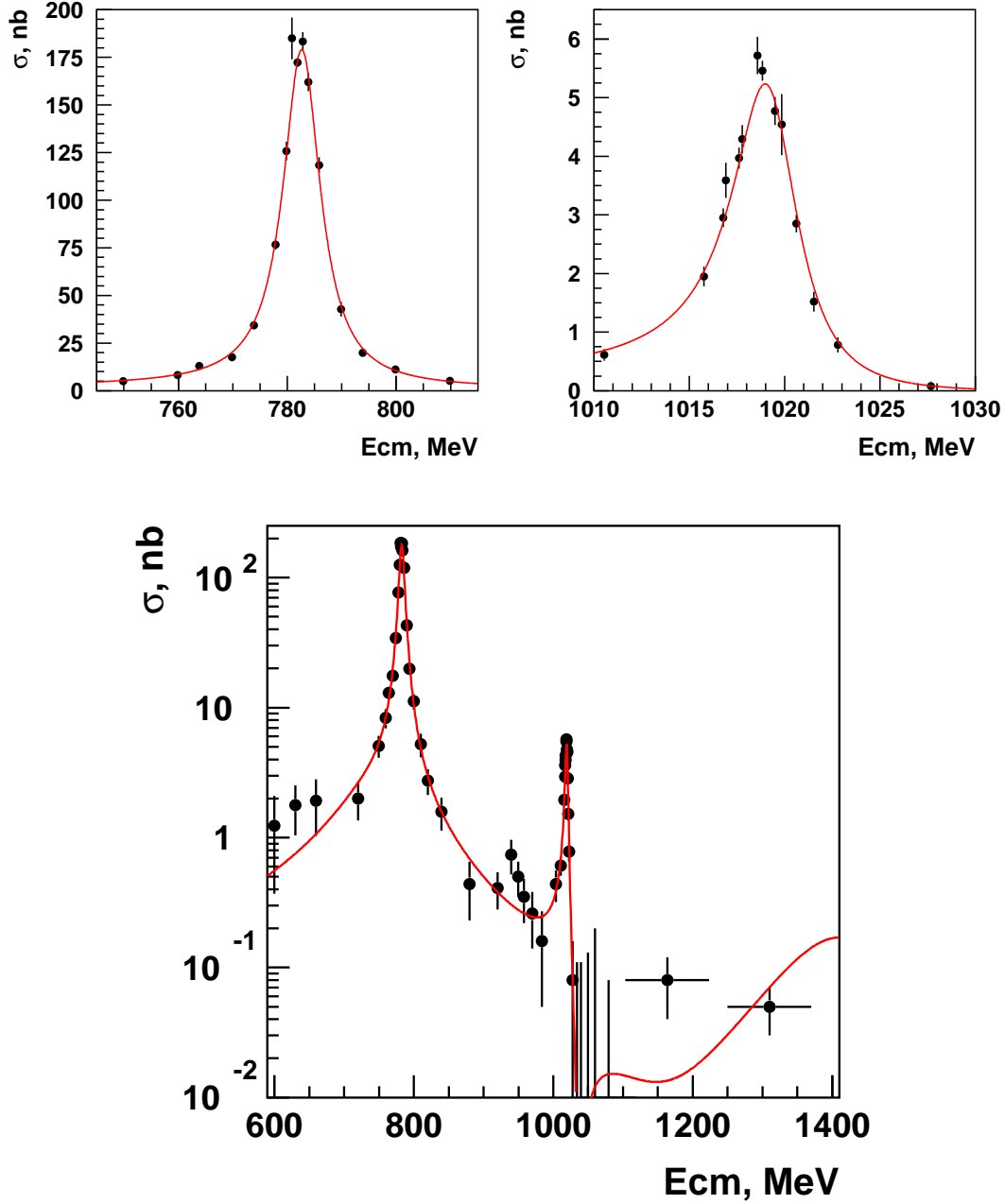


Fig. 5. The cross section of the process  $e^+e^- \rightarrow \pi^0\gamma$ . The points with error bars represent the experimental data, the curve corresponds to the result of the fit.

respectively,  $\delta_V$  is its relative phase,  $F(s)$  is a factor taking into account the energy dependence of the phase space of the final state,  $F_{P\gamma}(s) = p_\gamma^3 = (\sqrt{s}(1 - m_P^2/2s))^3$ ,  $\sigma_V^{(0)}$  is the cross section at the resonance peak:

$$\sigma_V^{(0)} = \sigma_{e^+e^- \rightarrow V \rightarrow \eta\gamma}(m_V^2) = \frac{12\pi B_{V \rightarrow e^+e^-} B_{V \rightarrow \eta\gamma}}{m_V^2}, \quad (3)$$

Table 5

Results of the fits for the processes  $e^+e^- \rightarrow \eta\gamma$  and  $e^+e^- \rightarrow \pi^0\gamma$ 

Parameter	$\eta\gamma$	$\pi^0\gamma$
$\sigma_\rho^{(0)}$ , nb	$0.145 \pm 0.063$	$0.708_{-0.134}^{+0.146}$
$\sigma_\omega^{(0)}$ , nb	$0.299_{-0.124}^{+0.175}$	$154.82_{-3.24}^{+3.29}$
$\sigma_\phi^{(0)}$ , nb	$22.791_{-0.238}^{+0.220}$	$5.30 \pm 0.16$
$\sigma_{\omega'}^{(0)}$ , nb	–	$0.139_{-0.051}^{+0.048}$
$m_\phi$ , MeV	$1019.52 \pm 0.05$	1019.46 (fixed)
$m_\omega$ , MeV	782.59 (fixed)	$783.20 \pm 0.13$
$\varphi_{\phi-\omega}$ , $^\circ$	180 (fixed)	$164.4 \pm 7.9$
$\chi^2/\text{n.d.f.}$	72.3/82	74.0/80

where  $B_{V \rightarrow e^+e^-}$  and  $B_{V \rightarrow \eta\gamma}$  are the corresponding branching ratios. In Eq. (2) we sum over all vector mesons relevant at this energy,  $V = \rho, \omega, \phi, \rho', \omega'$ .

The Gounaris-Sakurai model has been used for the description of the  $\rho$  meson [27]. To describe the energy dependence of the  $\omega$  and  $\phi$  meson widths, their main decay modes  $\pi^+\pi^-\pi^0$ ,  $\pi^0\gamma$  as well as  $K_L^0 K_S^0$ ,  $K^+K^-$ ,  $\pi^+\pi^-\pi^0$  and  $\eta\gamma$ , respectively, were taken into account using the same parameterization as in [28]. For the  $\rho'(1450)$  the energy dependence of the width assumed 60% and 40% branching ratios for its decays into  $a_1(1260)\pi$  and  $\omega\pi$ , respectively [29]. Its mass and width were taken to be 1465 MeV and 400 MeV, respectively [12]. The energy dependence of the  $\omega'(1420)$  width is calculated assuming the  $\omega' \rightarrow \rho\pi$  decay. Its mass and width were fixed at the world average values of 1425 MeV and 215 MeV, respectively [12].

### 3.2 Results of the fits

For the fit to the  $e^+e^- \rightarrow \eta\gamma$  cross section the resonance cross sections at the peak  $\sigma_\rho^{(0)}$ ,  $\sigma_\omega^{(0)}$ ,  $\sigma_\phi^{(0)}$  as well as the  $\phi$  meson mass  $m_\phi$  are free parameters. The  $\rho$  and  $\omega$  meson phases are chosen to be  $\varphi_\rho = \varphi_\omega = 0^\circ$  while that for the  $\phi$  meson is  $\varphi_\phi = 180^\circ$  in agreement with the quark model. The values of the other parameters are taken from Ref. [12]. We also consider a model in which in addition to the parameters described above there is a contribution tentatively referred to as that of the  $\rho'(1450)$  meson. A fit in the model with the  $\rho'(1450)$  doesn't improve  $\chi^2$  and results in the value of  $\sigma_{\rho'}^{(0)}$  consistent with zero,  $\sigma_{\rho'}^{(0)} = 0.001_{-0.001}^{+0.072}$  nb and compatible with our result in the  $3\pi^0$  mode [20]  $\sigma_{\rho'}^{(0)} = 0.066 \pm 0.015$  nb. Therefore, for our final results for the  $\eta\gamma$  decay we choose a model where  $\sigma_{\rho'}^0 = 0$  nb, see Table 5.

For the  $e^+e^- \rightarrow \pi^0\gamma$  case the fit parameters are: the cross sections at the resonance peak  $\sigma_\rho^{(0)}$ ,  $\sigma_\omega^{(0)}$ ,  $\sigma_\phi^{(0)}$  and the  $\omega$  meson mass  $m_\omega$ . The  $\rho-\omega$  phase is fixed to the value  $13.3^\circ$  obtained in our study of the process  $e^+e^- \rightarrow \pi^+\pi^-$  [26]. The  $\phi-\omega$  phase is a fit parameter. A fit, which includes a possible  $\omega'$  contribution, gives the best  $\chi^2$  at the value of  $\sigma_{\omega'}^{(0)}$  significantly differing from zero. Results of the best fit are shown in the last column of Table 5.

### 3.3 Systematic errors

There are two types of systematic uncertainties on the cross section  $\sigma_V^0$ : experimental and model uncertainties. The main sources of experimental systematic errors are listed below. The systematic error due to selection criteria is 4% estimated by varying the photon energy threshold, total energy deposition, total momentum, and  $\chi^2$ . A possible uncertainty because of the method of process separation was estimated to be 3% by comparing our results obtained from fitting the distributions of the two-photon invariant mass to those from Dalitz plot analysis. The latter method also allows to determine the cross section of the QED process  $e^+e^- \rightarrow 3\gamma$  and it appears to be consistent with the theoretical prediction [30]:  $\sigma(3\gamma)_{\text{exp}}/\sigma(3\gamma)_{\text{th}} = 0.973 \pm 0.018$ . The uncertainty in the determination of the integrated luminosity is 1% and comes from the selection criteria of Bhabha events, radiative corrections and calibrations of DC and BC. The error of the NT efficiency was estimated to be 2% by trying various fitting functions for energy dependence and variations of the cluster threshold. The 1% uncertainty of the radiative corrections comes from the dependence on the emitted photon energy and the accuracy of the theoretical formulae. In total, the experimental systematic uncertainty of the cross section is 6%.

The model uncertainty estimated by comparing the values of the cross section at the resonance peak in various models differing by the values of phases and resonance parameters was 1% (2%) for the  $\rho$ , 3%(0.1%) for the  $\omega$  and 0.1%(5%) for the  $\phi$  meson in the  $\eta\gamma$  and  $\pi^0\gamma$  decay modes, respectively.

## 4 Discussion

In Table 6 we present our results in terms of the product of the branching ratios  $\mathcal{B}(V \rightarrow e^+e^-) \times \mathcal{B}(V \rightarrow P\gamma)$ , where  $P = \eta(\pi^0)$ , which is calculated from  $\sigma_V^{(0)}$  according to (3). For the  $\eta\gamma$  mode one should additionally take into account the branching ratio of the  $\eta \rightarrow \gamma\gamma$  decay taking its value  $\mathcal{B}(\eta \rightarrow \gamma\gamma) = (39.43 \pm 0.26)\%$  from Ref. [12]. For the  $\pi^0\gamma$  mode the corresponding value  $\mathcal{B}(\pi^0 \rightarrow \gamma\gamma) = (98.798 \pm 0.032)\%$  from Ref. [12] was included at the MC

Table 6

 $\mathcal{B}(V \rightarrow e^+e^-) \times \mathcal{B}(V \rightarrow P\gamma)$ 

Decay	This work	PDG-2004
$\rho \rightarrow \eta\gamma, 10^{-8}$	$1.50 \pm 0.65 \pm 0.09$	$1.38 \pm 0.17$
$\omega \rightarrow \eta\gamma, 10^{-8}$	$3.17_{-1.31}^{+1.85} \pm 0.21$	$3.53 \pm 0.35$
$\phi \rightarrow \eta\gamma, 10^{-6}$	$4.093_{-0.043}^{+0.040} \pm 0.247$	$3.85 \pm 0.07$
$\rho \rightarrow \pi^0\gamma, 10^{-8}$	$2.90_{-0.55}^{+0.60} \pm 0.18$	$2.8 \pm 0.6$
$\omega \rightarrow \pi^0\gamma, 10^{-6}$	$6.47 \pm 0.14 \pm 0.39$	$6.37_{-0.15}^{+0.17}$
$\phi \rightarrow \pi^0\gamma, 10^{-7}$	$3.75 \pm 0.11 \pm 0.29$	$3.67 \pm 0.28$

Table 7

 $\mathcal{B}(V \rightarrow P\gamma)$ 

Decay	This work	PDG-2004
$\rho \rightarrow \eta\gamma, 10^{-4}$	$3.21 \pm 1.39 \pm 0.20$	$3.0 \pm 0.4$
$\omega \rightarrow \eta\gamma, 10^{-4}$	$4.44_{-1.83}^{+2.59} \pm 0.28$	$4.9 \pm 0.5$
$\phi \rightarrow \eta\gamma, 10^{-2}$	$1.373 \pm 0.014 \pm 0.085$	$1.295 \pm 0.025$
$\rho \rightarrow \pi^0\gamma, 10^{-4}$	$6.21_{-1.18}^{+1.28} \pm 0.39$	$6.0 \pm 1.3$
$\omega \rightarrow \pi^0\gamma, 10^{-2}$	$9.06 \pm 0.20 \pm 0.57$	$8.92_{-0.24}^{+0.28}$
$\phi \rightarrow \pi^0\gamma, 10^{-3}$	$1.258 \pm 0.037 \pm 0.077$	$1.23 \pm 0.10$

generation stage. Our results are in good agreement with the world average values [12].

By dividing the product of the branching ratios above by the corresponding world average leptonic width from Ref. [12] one can obtain the branching ratios of the radiative decays confronted in Table 7 to the world average values [12].

Taking into account a variation of the  $m_\omega$  and  $m_\phi$  in various models as well as a systematic error caused by the uncertainties of the beam energy calibration, we obtain for the resonance masses:

$$m_\omega = 783.20 \pm 0.13 \pm 0.16 \text{ MeV}, \quad (4)$$

$$m_\phi = 1019.52 \pm 0.05 \pm 0.05 \text{ MeV}, \quad (5)$$

consistent with the world average values  $782.59 \pm 0.11 \text{ MeV}$  and  $1019.456 \pm 0.020 \text{ MeV}$ , respectively [12].

Our result for the cross section of the process  $e^+e^- \rightarrow \eta\gamma$  at the peak of the  $\phi$  meson can be combined with the independent measurement of the same

quantity in the decay mode  $\eta \rightarrow 3\pi^0$  performed at CMD-2 [20] to obtain the ratio of the branching fractions of the  $\eta$  meson,  $\mathcal{B}(\eta \rightarrow 3\pi^0)/\mathcal{B}(\eta \rightarrow \gamma\gamma)$ . Since in both cases the  $\eta$  meson decays into neutral particles only, most of systematic uncertainties will cancel in such a ratio. As a result, two sources of the systematic error survive: 2.5% for the selection criteria and 3% due to process separation and we obtain

$$\frac{\mathcal{B}(\eta \rightarrow 3\pi^0)}{\mathcal{B}(\eta \rightarrow \gamma\gamma)} = 0.817 \pm 0.012 \pm 0.032, \quad (6)$$

which is consistent with the world average value  $0.825 \pm 0.007$  [12].

## 5 Conclusions

- Using a data sample corresponding to integrated luminosity of  $21 \text{ pb}^{-1}$ , the cross sections of the processes  $e^+e^- \rightarrow \eta\gamma, \pi^0\gamma$  have been measured in the c.m. energy range 600–1380 MeV. The following branching ratios have been determined:

$$\begin{aligned} \mathcal{B}(\rho^0 \rightarrow \eta\gamma) &= (3.21 \pm 1.39 \pm 0.20) \cdot 10^{-4}, \\ \mathcal{B}(\omega \rightarrow \eta\gamma) &= (4.44_{-1.83}^{+2.59} \pm 0.28) \cdot 10^{-4}, \\ \mathcal{B}(\phi \rightarrow \eta\gamma) &= (1.373 \pm 0.014 \pm 0.085) \cdot 10^{-2}, \\ \mathcal{B}(\rho^0 \rightarrow \pi^0\gamma) &= (6.21_{-1.18}^{+1.28} \pm 0.39) \cdot 10^{-4}, \\ \mathcal{B}(\omega \rightarrow \pi^0\gamma) &= (9.06 \pm 0.20 \pm 0.57) \cdot 10^{-2}, \\ \mathcal{B}(\phi \rightarrow \pi^0\gamma) &= (1.258 \pm 0.037 \pm 0.077) \cdot 10^{-4}. \end{aligned}$$

- From the two independent measurements of the  $\phi \rightarrow \eta\gamma$  decay the following ratio of the branching ratios of the  $\eta$  meson has been obtained:

$$\mathcal{B}(\eta \rightarrow 3\pi^0)/\mathcal{B}(\eta \rightarrow \gamma\gamma) = 0.817 \pm 0.012 \pm 0.032.$$

## Acknowledgments

The authors are grateful to the staff of VEPP-2M for the excellent performance of the collider, and to all engineers and technicians who participated in the design, commissioning and operation of CMD-2. This work is supported in part by grants DOE DEFG0291ER40646, NSF PHY-0100468, PST.CLG.980342, RFBR-03-02-16280, RFBR-03-02-16477, RFBR-03-02-16843, RFBR-04-02-16217, and RFBR-04-02-16223-a.



## References

- [1] T. Ohshima, Phys. Rev. D 22 (1980) 707.
- [2] P.J. O'Donnell, Rev. Mod. Phys. 53 (1981) 673.
- [3] A. Bramon, A. Grau, G. Pancheri, Phys. Lett. B 344 (1995) 240.
- [4] M. Hashimoto, Phys. Rev. D 54 (1996) 5611.
- [5] M. Benayoun, S.I. Eidelman, V.N. Ivanchenko, Z. Phys. C 72 (1996) 221.
- [6] P. Ball, J.M. Frere, M. Tytgat, Phys. Lett. B 365 (1996) 367.
- [7] A. Bramon, R. Escribano, M.D. Scadron, Eur. Phys. J. C 7 (1999) 271.
- [8] M. Benayoun, Phys. Rev. D 59 (1999) 114027.
- [9] M. Davier, et al., Eur. Phys. J. C 31 (2003) 503.
- [10] T. Barnes, et al., Phys. Rev. D 55 (1997) 4157.
- [11] F. Close, A. Donnachie, Yu.S. Kalashnikova, Phys. Rev. D 67 (2003) 074031.
- [12] S. Eidelman et al., Phys. Lett. B 592 (2004) 1.
- [13] V.P. Druzhinin, et al., Phys. Lett. 144 B (1984) 136.
- [14] S.I. Dolinsky et al., Z. Phys. C42 (1989) 511.
- [15] M.N. Achasov et al., Eur. Phys. J. C 12 (2000) 25.
- [16] M.N. Achasov et al., Phys. Lett. B 559 (2003) 171.
- [17] G. A. Aksenov et al., Preprint Budker INP 85-118, Novosibirsk, 1985;  
E. V. Anashkin et al., ICFA Instr. Bulletin 5 (1988) 18.
- [18] R. R. Akhmetshin et al., Preprint Budker INP 99-11, Novosibirsk, 1999.
- [19] E.V. Anashkin et al., Preprint Budker INP 99-1, Novosibirsk, 1999.
- [20] R.R. Akhmetshin et al., Phys. Lett. B 509 (2001) 217.
- [21] R.R. Akhmetshin et al., Phys. Lett. B 508 (2001) 217.
- [22] R.R. Akhmetshin et al., Phys. Lett. B 551 (2003) 27.
- [23] R.R. Akhmetshin et al., Phys. Lett. B 562 (2003) 173.
- [24] R.R. Akhmetshin et al., Phys. Lett. B 580 (2004) 119.
- [25] E. A. Kuraev and V.S. Fadin, Sov. J. Nucl. Phys., 41 (1985) 466.
- [26] R.R. Akhmetshin et al., Phys. Lett. B 578 (2004) 285.
- [27] G. J. Gounaris and J.J. Sakurai, Phys. Rev. Lett. 21 (1968) 244.

- [28] R.R. Akhmetshin et al., Phys. Lett. B 434 (1998) 426.
- [29] R.R. Akhmetshin et al., Phys. Lett. B 466 (1999) 392.
- [30] S.I. Eidelman and E.A. Kuraev, Nucl. Phys. B 143 (1978) 353.